

Article

## Structural and Electrochemical Properties of Binary ZnO:Al Nanocomposites as Anode for Lithium-ion Batteries

Maisurah Mukhtar<sup>1</sup>, Najiha Hamid<sup>1</sup>, Syahida Suhaimi<sup>1</sup>,  
Azwani Sofia Ahmad Khair<sup>1</sup>, Nur Athirah Mohd Taib<sup>1</sup> and  
Peshawa Omer Amin<sup>2</sup>

<sup>1</sup>Faculty of Science and Technology, Universiti Sains Islam Malaysia, Bandar Baru Nilai, 71800 Nilai, Negeri Sembilan, Malaysia.

<sup>2</sup>Department of Natural Science, Charmo Center for Research, Training and Consultancy, Charmo University, Chamchamal 46023, Iraq.

Correspondence should be addressed to:  
Syahida Suhaimi; syahida@usim.edu.my

### Article Info

Article history:

Received: 7 May 2024

Accepted: 1 August 2024

Published: 7 October 2024

Academic Editor:

Mohd Hafiz Abu Hassan

Malaysian Journal of Science, Health & Technology

MJoSHT2024, Volume 10, Issue No. 2

eISSN: 2601-0003

<https://doi.org/10.33102/mjosht.v10i2.420>

Copyright © 2024 Maisurah Mukhtar et al.

This is an open access article distributed under the Creative Commons Attribution 4.0 International License, which permits unrestricted use, distribution, and reproduction in any medium, provided the original work is properly cited.

**Abstract**— In conventional lithium-ion batteries (LIBs), carbon compounds are commonly utilised as the anode owing to their great performance, low cost, and abundance. However, due to the limited storage capability of pure carbon materials that restrict further improvement of LIBs, zinc oxide (ZnO) has been one of the promising anode materials to be used as an alternative to strengthen the electrochemical performance of LIBs due to its high theoretical capacity of 987 mAh g<sup>-1</sup>. This study aims to synthesise ZnO:Al nanowires using the hot-tube thermal evaporation method. Three types of samples are made using this method by varying the concentration of 0 wt% (S1), 3wt% (S2), and 6 wt% (S3) of aluminium (Al) during the Al deposition process. The EDX findings indicated that the sample has a high proportion of zinc (Zn) and oxygen (O), with the S3 sample having the highest Al concentration after being deposited. The most substantial diffraction peak for XRD of all samples was found at (101), exhibiting a single crystalline hexagonal structure with optimum growth direction on the c-axis. For EIS analysis, the S3 sample has the lowest bulk resistance and maximum ionic conductivity. In conclusion, the ZnO sample with 3 wt% of Al as a dopant was selected as the optimum result to synthesise a homogenous surface of ZnO:Al with good crystallinity by using a hot-tube thermal evaporation process and giving the best conductivity in electrochemical performance.

**Keywords**— zinc oxide; aluminium; thermal evaporation technique; nanostructures; anode

### I. INTRODUCTION

Lithium-ion batteries are expected to continue the domination of batteries and may even overshadow gasoline-powered technologies in the future [1]. Owing to their high performance, reliability, and extensive lifespan, lithium-ion batteries have been the most promising electrochemical power supply devices. They have the ability to securely store huge amounts of energy, providing reliable and predictable electrical flows even in decentralised static or mobile modes in distant places [2][3].

As an important component of LIBs, the commonly used graphite anodes have encountered some technical limitations, one of which is their inability to satisfy the extensive demands of high energy and power densities due to their relatively low lithium theoretical storage capacity of only 372 mAh g<sup>-1</sup> [2][4]. In excess of what has been stipulated, LIBs are often seen as being the least-green components of any electronic device due to their dependency on graphite anode [5].

Along with this issue, it is speculated that there are two viable techniques for increasing the capacity of carbon-based materials without increasing their amounts and one of the

options is to shrink the size of carbon down to the nanoscale or introduce pores into the carbon structure, which can convey additional active sites for storing lithium ions while also facilitating their kinetic process. However, despite the fact that carbon-based nanoparticles, nanowires, and nanosheets do possess high reversible capacities, their voltage output is unstable [6].

In recent studies, zinc oxide (ZnO) has been proposed as a potential alternative anode to graphite, which is currently used due to its high theoretical capacity of  $978 \text{ mAh g}^{-1}$ , greater lithium-ion diffusion coefficient, and natural abundance. However, despite the potential of ZnO as an anode material, its practical application is hampered by intrinsic challenges such as poor electrical conductivity and significant volume changes during charge-discharge cycles, leading to rapid capacity fading and reduced battery life [7].

On the other hand, studies have indicated that the electrical and electrochemical characteristics of ZnO can be enhanced through doping with hetero-elements. Specifically, when elements such as aluminium, gallium, and indium are introduced as dopants, the electrical conductivity of ZnO undergoes significant improvement [8][9]. Based on these findings, it is reasonable to consider Al-doped ZnO nanostructures as promising candidates for anode materials in LIBs.

On the basis of this, this study is done on the desire to develop a facile approach to synthesising ZnO composite embedded with aluminium nanostructures (ZnO:Al) using the hot-tube thermal evaporation (HTTE) method to demonstrate that ZnO:Al is a potential anode material for lithium-ion batteries.

## II. THE MATERIAL AND METHOD

### A. Materials

The materials used in this study include high purity (99.99%) zinc powder (Zn) and aluminium powder (Al) obtained from Sigma-Aldrich, USA. Silicon substrates (Si) were sourced from SiTerra Malaysia Sdn. Bhd., Malaysia. High purity (99.999%) argon (Ar) and oxygen ( $\text{O}_2$ ) gases were supplied by Malaysian Oxygen Berhad (MOX), Malaysia.

### B. Fabrication of ZnO Nanowires and Al Deposition

The process was done in the furnace tube of the hot-tube thermal evaporation system, as shown in Figure 1. Commercially available high-purity metallic zinc powder (99.99%) was used as a precursor of ZnO. About 1g of the Zn powder was weighed and put into an alumina boat positioned at the centre of the quartz tube furnace. The silicon (Si) substrate at a tilt angle of  $30^\circ$  was then placed in the furnace tube at a distance of 18 cm from the alumina boat.

As the furnace reaches a vacuum state, a carrier gas (Ar) acting as a carrier gas was introduced at a flow rate of 75%, while oxygen gas ( $\text{O}_2$ ) at a 25% flow rate was introduced once the  $800^\circ\text{C}$  temperature was reached for 150 minutes. The Zn was vapourised slowly in the growth process, and once the process was completed after 150 minutes, the sample of ZnO nanowires was obtained and taken out to proceed with aluminium deposition for the fabrication of ZnO:Al.

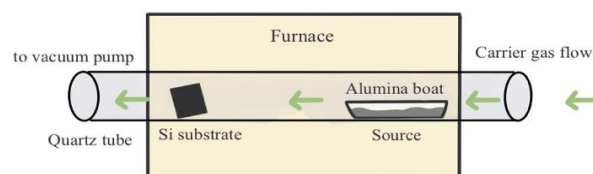


Fig. 1 Schematic diagram of reaction in the furnace and quartz tube during the thermal evaporation process

The ZnO precursor was then introduced to the aluminium deposition process by undergoing the same hot tube thermal evaporation technique, as illustrated in Figure 2. The sample of ZnO nanowires on the Si substrate obtained from the previous step was placed into the sample holder. Aluminium powder was then weighed at different mass percentages (0%, 3%, and 6%) and placed in the alumina boat. The substrate was placed in the furnace tube with a tilt angle set at  $30^\circ$ . The growth process was then proceeded using the same step with the same pressure and temperature setup. These deposited products on Si  $\langle 100 \rangle$  substrates were then finally examined in terms of their structural and electrochemical properties. Table I summarises the number of samples fabricated and their modifications.

TABLE I. COMPOSITION AND DETAIL OF FABRICATED SAMPLES

No.	Sample name	Sample details
1	S1	ZnO:Al nanocomposites with 0 wt% Al
2	S2	ZnO:Al nanocomposites with 3 wt% Al
3	S3	ZnO:Al nanocomposites with 6 wt% Al

### C. Hot-tube Thermal Evaporation Setup

Both processes of synthesising ZnO nanowires and their Al deposition involve thermal evaporation techniques. The hot-tube thermal evaporation system was set up using a horizontal-tube furnace reactor based on Figure 2. The system includes the power source, temperature controller, thermocouple, tube furnace, flow meters, pressure gauge, rotary pump, and a variety of valves. The mass flow controllers (or thermal mass flow meter) for oxygen and argon gas are essential to regulate the gas flow rate based on a predetermined flow rate without being impacted by alterations in the gas pressure. The pressure gauge, diaphragm valve, and up-to-air valve are attached to a rotary vacuum pump to determine the pressure and enable the compression of air inside the chamber. A thermocouple is also connected to sense temperature by corresponding to a voltage. Both mass flow controllers, the vacuum pump, the valves, and the thermocouple are all connected to the quartz tube.

$$D = \frac{K\lambda}{\beta \cos\theta} \quad (4)$$

- $D$  : Crystallite size  
 $K$  : 0.9 (constant)  
 $\lambda$  : Mean wavelength of Cu  $K\alpha$  radiation (0.154056 nm)  
 $\beta$  : Full-width half maximum (FWHM) of Bragg peak observed at angle  $\theta$  (rad)

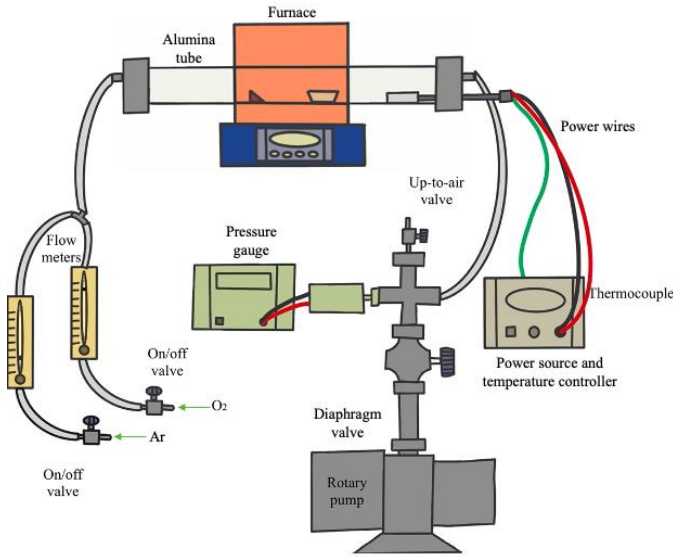


Fig. 2. Schematic diagram of hot-tube thermal evaporation system

#### D. Characterisation of Synthesised ZnO:Al Nanocomposites Anode

For imaging and analysis, a JEOL IT800 Field Emission Scanning Electron Microscopy (FESEM) from JEOL Ltd., Japan, was used, operating at 5 kV with magnification ranging from 50,000X to 200,000X [10]. To enhance the analysis of the tapering degree, the Tapering Factor ( $TF$ ) was also measured. The lowest  $TF$  value is zero (0.00), suggesting that the width along the nanowire is consistent, while a higher  $TF$  value implies a bigger deviation diameter. The  $TF$  value may be calculated using Equation 3.

$$d_i = \frac{dT_i + dM_i + dB_i}{3} \quad (1)$$

$$TF_i = \frac{|dT_i - d_i| + |dM_i - d_i| + |dB_i - d_i|}{3} \quad (2)$$

$$TF = \sum_{i=1}^n \frac{TF_i}{n} \quad (3)$$

- $TF$  : Tapering factor ( $TF \geq 0.00$ )  
 $TF_i$  : Tapering factor of individual nanowire  
 $n$  : The number of nanowire samples  
 $d_i$  : Average diameter of individual nanowire  
 $dT_i$  : Diameter of the tip part of the nanowire  
 $dM_i$  : Diameter of the middle part of the nanowire  
 $dB_i$  : Diameter of the bottom part of the nanowire

Energy Dispersive X-ray (EDX) analysis was also integrated with the JEOL IT800 FESEM [11]. X-ray Diffraction (XRD) was performed using a MiniFlex Rigaku from Rigaku Corporation, Japan, operating at 40 kV and 30 mA with Cu  $K\alpha$  radiation ( $\lambda = 1.5406 \text{ \AA}$ ) [12]. In Equation 4, the crystalline size ( $D$ ) of the films was computed using the plane of the Zincite phase and Scherrer's equation.

$$\sigma = \frac{t}{AR_b} \quad (5)$$

- $t$  : Thickness of the sample  
 $A$  : Cross-sectional area of the sample  
 $R_b$  : Bulk resistance

### III. RESULTS AND DISCUSSION

#### A. Field Emission Scanning Electron Microscopy (FESEM) Analysis

The FESEM images of all samples examined are shown in Figure 3. The analysis shows that the ZnO:Al nanostructures are dispersed and distributed evenly across the surface of the Si substrate with varying Al concentrations of 0 wt% (S1) and 3 wt% (S2), as shown in Figure 3(a), 3(b), 3(c), and 3(d), respectively, except for sample S3 with Al concentration of 6 wt% as shown in Figure 3(e) and 3(f). All three different samples have three different morphologies, demonstrating that Al concentration significantly impacts the structural properties.

Based on Figure 3(a) and 3(b), sample S1 of pure ZnO nanowires seemed to be randomly orientated in general. Most ZnO nanowires have a high aspect ratio, with diameters ranging from 40 to 50 nm and lengths ranging from 100 to 200 nm. Based on the images, this simple HTTE procedure is a viable option for ZnO nanowire synthesis. As there is no catalyst employed in the growth procedures, no catalyst particles are detected at the ZnO nanowire tips. Hence, the formation of straight nanowires of ZnO depicted here may occur from the vapour-solid (VS) mechanism [15].

In Figures 3(c) and 3(d), the impact of Al as a dopant is observable on the wall of ZnO as 3 wt% of Al is deposited on ZnO nanowires. Sample S2 also appeared to be haphazardly oriented. In contrast to the nanoneedle structure in the undoped ZnO nanowires, sample S2 looked to display growth like a button mushroom. Furthermore, unforeseen properties in images of Al-doped samples are equivalent to those in images of undoped ZnO nanowires. The nanowires seemed to have diameters ranging from 180 to 220 nm and lengths

ranging from 400 to 600 nm. These widths and lengths are almost four times higher than those of undoped ZnO nanowires, and this might be clarified by the doping effect in ZnO nanostructures. Compared to other figures, the length and diameters of ZnO nanostructures in Figure 3(c) are the greatest. Hence, it can be concluded that sample S2 is the most optimum sample as it has the biggest area for any reaction to occur.

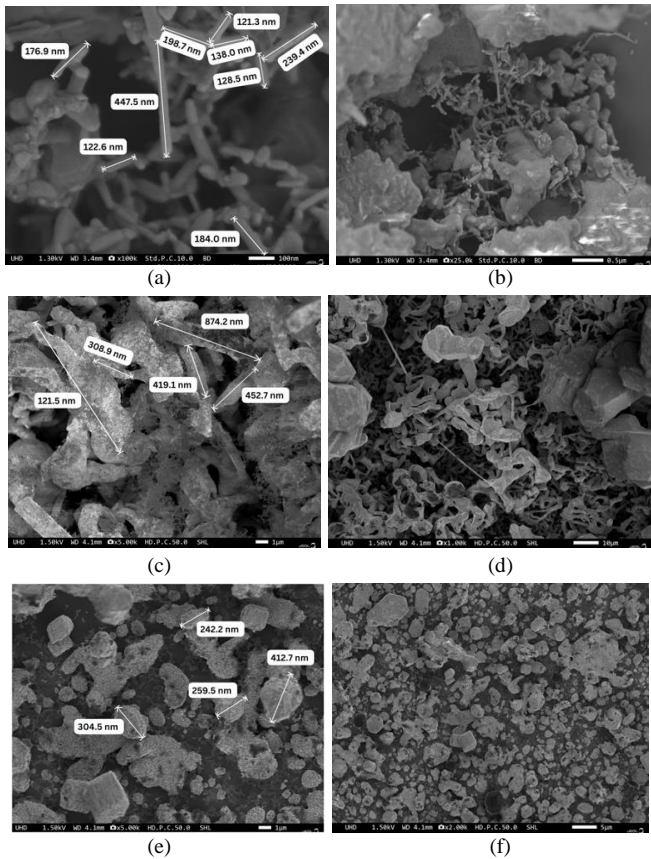


Fig. 3 FESEM images of (a) S1 at 100.00 kX magnification (b) S1 at 25.00 kX magnification (c) S2 at 5.00 kX magnification (d) S2 at 1.00 kX magnification (e) S3 at 5.00 kX magnification and (f) S3 at 2.00 kX magnification

In Figures 3(e) and 3(f), the increasing Al concentration to 6 wt% as a dopant for ZnO nanowires clearly shows that the morphology of the nanostructures was broken, irregular, and gave the form of an intact round shape. The structures also decrease to approximately 300 nm in length and 110 to 130 nm in diameter. Although the length and diameter of sample S3 were greater than the undoped ZnO nanowires, it seems that S3 had shown an agglomeration with the addition of a dopant concentration of 6 wt% Al. The agglomeration observed may be attributed to the increased surface defects. The addition of 6% Al likely induces more defects and strain within the ZnO lattice, which can act as nucleation points for agglomeration. The emergence of these defects creates regions of higher energy levels, causing the nanowires to cluster together to achieve a more stable state [16][17].

Table II describes the overall length and width on the tip, middle, and bottom, including the tapering factor of ZnO nanowires generated with different Al concentrations as dopants. The tapering factor for sample S2, with a value of

1.36, has the closest value to 0.00 among other samples – suggesting that the nanowires of S2 are the most uniform. Thus, it was determined that varying Al concentration as a dopant significantly influenced the nucleation and development of ZnO nanostructures.

TABLE III. SUMMARY OF AVERAGE LENGTH AND DIAMETER ON THE TIP, MIDDLE, AND BOTTOM, AND TAPERING FACTOR OF ZINC OXIDE NANOWIRES WITH VARYING CONCENTRATIONS OF ALUMINIUM

Sample	Average length (nm)	dT (nm)	dM (nm)	dB (nm)	TF
S1	215.7	40.9	43.0	45.7	1.66
S2	435.3	214.0	183.0	182.8	1.36
S3	304.7	112.7	129.2	130.8	7.70

### B. Morphology Analysis by Energy Dispersive X-ray (EDX)

The elements included in the synthesised pure ZnO and ZnO:Al nanowires were determined using EDX. Figure 4 depicts the EDX spectra of samples S1, S2, and S3, respectively. It can be concluded that the zinc (Zn) element has dominated the content in nanostructures, followed by oxygen (O) and carbon (C). The result indicates that the ZnO nanowires produced are of high quality. The presence of carbon in each sample may result from the furnace's heating process. The element of sodium (Na) could have come from the material of the substrate, while the element of aluminium (Al) in pure ZnO nanowires, as depicted in Figure 4(a), may come from the material of alumina boat, which was used as the source holder.

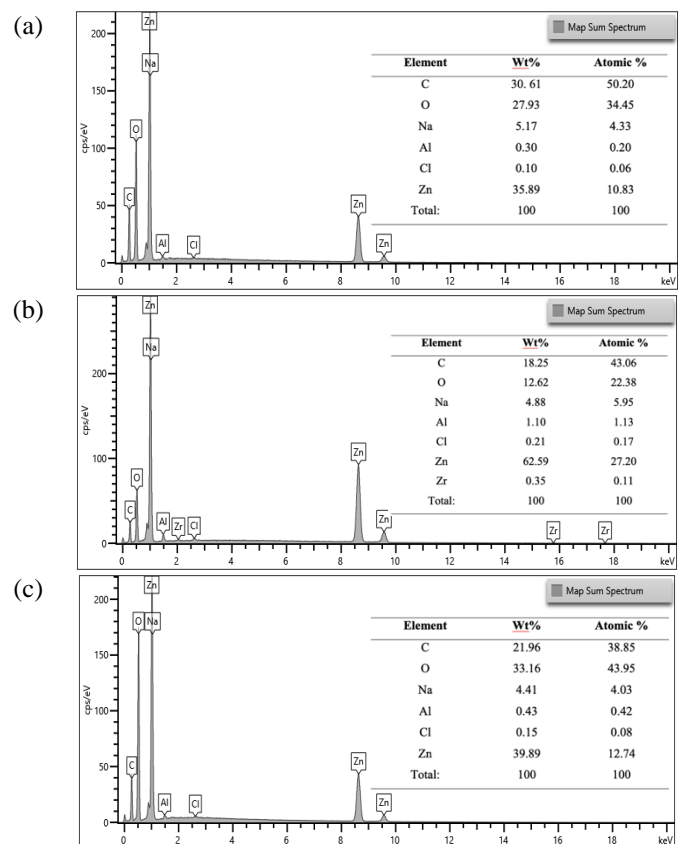


Fig. 4 EDX Spectra OF ZnO nanostructure doped with different Al concentrations of (a) 0 wt% (b) 3 wt% (c) 6 wt%

Although the element of Na in all samples is considerably high, it would not have much impact on the structural properties of the samples obtained. On the other hand, sample S2 has a higher percentage of Al element than sample S3, as illustrated in Figure 4(b) and Figure 4(c). It can be seen that the Al concentration in S3 is lower than S2 although the Al concentration used for S3 is higher. It may occur due to 6 wt% of Al concentration not being fully deposited onto the sample during the Al deposition process. Additionally, the insignificant amount of zirconium (Zr) element detected in sample S2, as shown in Figure 4(b), might come from the crucibles of the furnace linings.

Figure 5 illustrates the elemental mapping for all three samples with varied Al concentrations as dopants. It can be concluded from the figures that the elements are equally distributed and did not congregate in a single location, indicating that all samples exhibited excellent developed ZnO nanowires, although S3 possessed poor growth.

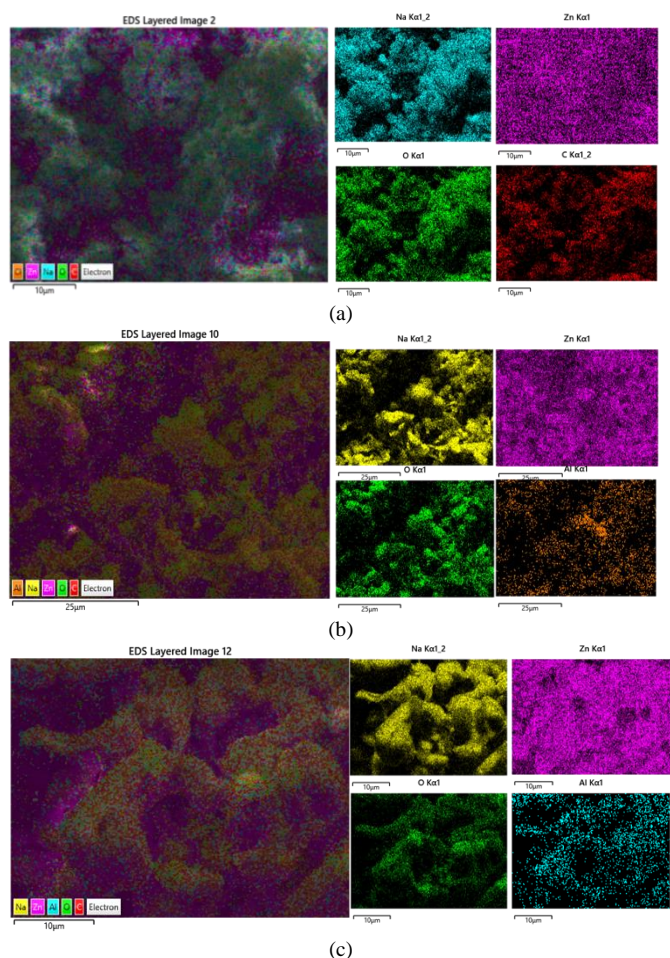


Fig. 5 EDX overall mapping and elemental mapping of the sample (a) S1 (b) S2, and (c) S3

### C. X-ray Diffraction (XRD) Analysis

The crystal structure of the ZnO nanostructure was determined using XRD analysis. Figure 6 depicts three XRD patterns representing all samples, which exhibit a few strong peaks due to high-purity ZnO nanocrystalline phases. The maximum peak for each sample was recorded with (101) orientation on the plane with a mean angle of  $2\theta \approx 36.24^\circ$ , as shown in the figure above. All observable peaks are

hexagonal wurtzite ZnO, compatible with the standard reference data *JCP2.2CA: 00-036-1451*. Furthermore, all samples had a very strong peak at the (101) plane, indicating that the synthesised ZnO was highly orientated, assuming *c*-axis growth perpendicular to the substrate surface, with the highly desirable *c*-axis orientation enhancing the final characteristics [18]. As a result, the Al content in ZnO nanowires influences the crystallinity of the ZnO, which involves the nucleation and growth process.

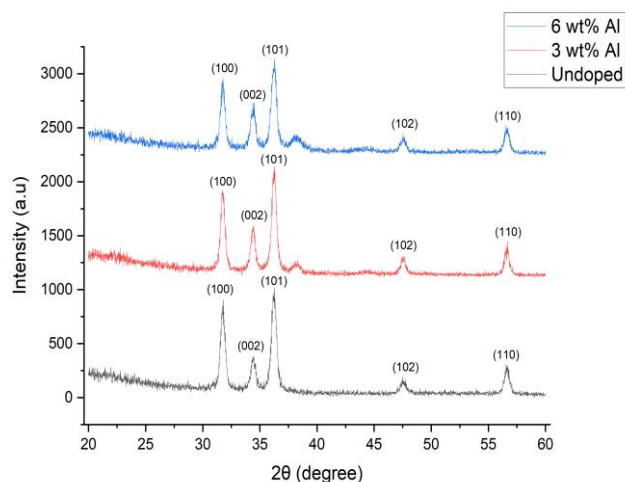


Fig. 6 XRD Spectra of all ZnO samples with varied Al concentration

The XRD data were then analysed further to determine the average crystallite size of the synthesised samples. Table III shows the average value of crystallite size for samples S1, S2, and S3. It could be seen that the value of *D* increases as the Al concentration increases but decreases when the Al concentration rises further to 6 wt%. The observed decrease in the *D* value for 6% aluminium-doped zinc oxide nanowires can be linked to the phenomenon of agglomeration, which results in the formation of larger nanoparticle clusters and influences the X-ray diffraction (XRD) patterns. The process of agglomeration leads to a noticeable broadening of the diffraction peaks. This effect makes the effective crystallite size seem smaller than it is. Essentially, when nanoparticles clump together, they create a more complex diffraction pattern where the individual contributions blur together, causing an overall broadening of the peaks [19]. Additionally, an increase in surface defects and strain within these clumped structures further amplifies this broadening effect by disturbing the otherwise regular arrangement of the crystal lattice, thus diminishing the perceived size of the crystallite [19][20].

TABLE III. MEASUREMENT AND STRUCTURAL CALCULATION OF ZINC OXIDE NANOWIRES WITH VARYING CONCENTRATION OF ALUMINIUM

Sample	<i>hkl</i> plane	Lattice spacing, <i>d</i>	$2\theta$ (°)	<i>a</i> (Å)	<i>c</i> (Å)	Crystallite size, <i>D</i> (nm)
S1	(101)	2.28	36.24	3.22	5.19	17.98
S2	(101)	5.68	36.25	8.04	8.04	19.82
S3	(101)	5.70	36.24	8.07	8.07	18.17

#### D. Electrochemical Impedance Spectroscopy (EIS) Analysis

In terms of electrochemical properties, S2 was chosen as the optimum sample based on its structural properties, which were analysed and tested for DC impedance. Bulk resistance,  $R_b$ , was obtained from the Nyquist plot and used to calculate the conductivity of samples S1 and S2 from the EIS conducted. The value of  $R_b$  was represented by the diameter of semicircles [14]. The Nyquist plot of sample S1 and S2 using EIS is shown in Figure 7.

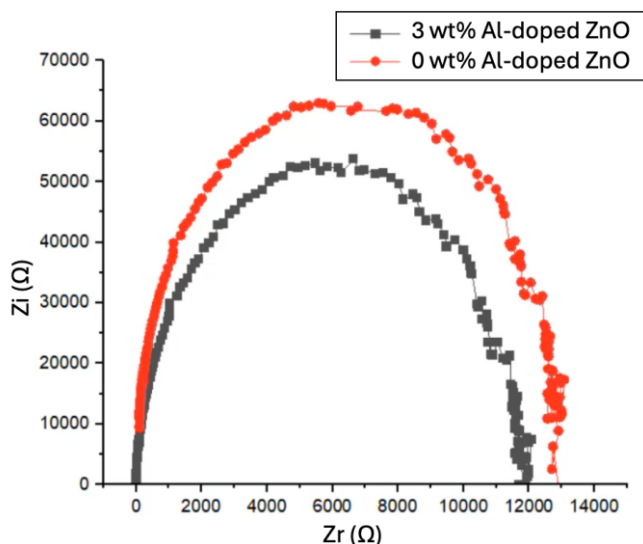


Fig. 7 The Nyquist plot of undoped ZnO nanowires (S1) and ZnO nanowires doped with 3 wt% of Al concentration (S2)

Table IV depicts the values corresponding to the resistance of both samples. It can be seen that the values decrease as the doped content increases, indicating that the pure ZnO nanowires sample has a greater impedance value than the 3 wt% of the Al-doped ZnO nanowires sample. As demonstrated in Figure 7, the impedance value lowers when Al ions are substituted in the ZnO lattice. Resistance reductions may be related to the increase in Al donor concentration caused by the replacement of  $Zn^{2+}$  sites in ZnO lattices with  $Al^{3+}$  ions [21].

TABLE IVV. MEASUREMENT AND STRUCTURAL CALCULATION OF ZINC OXIDE NANOWIRES WITH VARYING CONCENTRATION OF ALUMINIUM

Sample	Al concentration (wt%)	Resistance ( $\Omega$ )
S1	0	$1.29 \times 10^4$
S2	3	$1.19 \times 10^4$

Table V shows the ionic conductivity value for both samples.

TABLE V. MEASUREMENT AND STRUCTURAL CALCULATION OF ZINC OXIDE NANOWIRES WITH VARYING CONCENTRATION OF ALUMINIUM

Sample	Al concentration (wt%)	Ionic conductivity, $\sigma$ ( $S\text{cm}^{-1}$ )
S1	0	$1.34 \times 10^{-6}$
S2	3	$1.25 \times 10^{-6}$

From Table V, it can be concluded that the increase of Al doping in ZnO nanowires significantly increases ionic conductivity values. This behaviour may be caused by the addition of Al, which raises the free electron density by replacing Zn ions with Al ions, providing free electrons [22]. The replacement of  $Al^{3+}$  ions result in the production of one free electron for every  $Zn^{2+}$  ion, which enhances conductivity in the battery [22][23]. According to the EIS analysis, it can be concluded that Al-doped ZnO nanowires exhibited better conductivity and low resistance features than undoped ZnO nanowires, indicating potential applications in electrical devices.

#### IV. CONCLUSIONS

In this study, ZnO:Al nanowires were synthesised using the hot-tube thermal evaporation method at  $800^\circ\text{C}$  for 150 minutes, with varying Al concentrations of 0 wt% (S1), 3 wt% (S2), and 6 wt% (S3). The FESEM analysis revealed that the nanowires with 3 wt% Al doping were approximately 400 nm in length with a diameter ranging from 180 nm to 220 nm, larger than the undoped ZnO nanowires. This suggests that doping ZnO with 3 wt% Al results in superior structural properties. However, increasing the Al doping to 6 wt% led to agglomeration, resulting in irregular and fragmented nanowire structures. EDX analysis indicated a uniform distribution of Zn and O elements across the samples, confirming the formation of well-developed ZnO nanowires in all samples except for S3 (6wt% Al), which showed poor development of ZnO:Al nanowires. XRD patterns displayed characteristic hexagonal wurtzite ZnO peaks with a pronounced peak at the (101) plane, evidencing a high orientation of the synthesised ZnO. The 3 wt% Al-doped sample exhibited the largest nanowire size. These structural analyses suggest that the 3 wt% Al-doped ZnO nanowires represent the optimal composition. Electrochemically, EIS analysis showed that the 3 wt% Al-doped nanowires had lower bulk resistance and higher ionic conductivity compared to the undoped ZnO, indicating an enhancement in electrochemical performance for anode materials when doped with 3 wt% Al.

#### CONFLICT OF INTEREST

The authors declare that there is no conflict of interest regarding the publication of this paper.

#### ACKNOWLEDGEMENT

The authors would like to thank PI/FST/0121/USIM/15521 for funding this research and the Faculty of Science & Technology located at USIM for providing the laboratory with enough facilities throughout the experimental work.

#### REFERENCES

- [1] Motors. In IOP Conference Series: Earth and Environmental Science (Vol. 692, No. 2, p. 022103). IOP Publishing. <https://doi.org/10.1088/1755-1315/692/2/022103>

- [2] Tarascon, J. M., & Armand, M. (2001). Issues and challenges facing rechargeable lithium batteries. *nature*, 414(6861), 359-367. <https://doi.org/10.1038/35104644>
- [3] Liu, S. (2021). Competition and valuation: a case study of Tesla Motors. In *IOP Conference Series: Earth and Environmental Science* (Vol. 692, No. 2, p. 022103). IOP Publishing. <https://doi.org/10.1088/1755-1315/692/2/022103>
- [4] Hasegawa, K., Gunji, H., Kijima, R., Eguchi, M., Nishitani-Gamo, M., Ando, T., & Nakagawa, K. (2021). Electrochemical performance of marimocarbon/lithium titanate composites synthesized by hydrothermal method for lithium-ion batteries. *Journal of Materials Science*, 56, 16602-16611. <https://doi.org/10.1007/s10853-021-06319-w>
- [5] Huang, Y., Liu, X., Lu, L., Fang, J., Ni, H., & Ji, Z. (2015). Preparation and characterization of ZnO/SnO<sub>2</sub> composite thin films as high-capacity anode for lithium-ion batteries. *Applied Physics A*, 120, 519-524. <https://doi.org/10.1007/s00339-015-9209-x>
- [6] Xianlai Zeng, Jinhui Li & Narendra Singh (2014) Recycling of Spent Lithium-Ion Battery: A Critical Review, *Critical Reviews in Environmental Science and Technology*, 44:10, 1129-1165. <https://doi.org/10.1080/10643389.2013.763578>
- [7] Zhou, L., Yang, H., Han, T., Song, Y., Yang, G., & Li, L. (2022). Carbon-based modification materials for lithium-ion battery cathodes: Advances and perspectives. *Frontiers in Chemistry*, 10, 914930. <https://doi.org/10.3389/fchem.2022.914930>
- [8] Li, H., Liu, Z., Yang, S., Zhao, Y., Feng, Y., Bakenov, Z., Zhang, C. & Yin, F. (2017). Facile synthesis of ZnO nanoparticles on nitrogen-doped carbon nanotubes as high-performance anode material for lithium-ion batteries. *Materials*, 10(10), 1102. <https://doi.org/10.3390/ma10101102>
- [9] Norris, D. J., Efros, A. L., & Erwin, S. C. (2008). Doped nanocrystals. *Science*, 319(5871), 1776-1779. <https://doi.org/10.1126/science.1143802>
- [10] Zhang, L., Zhang, J., Liu, Y., & Guo, S. (2015). Effect of aluminium doping amount on the electrochemical properties of ZnO nanoparticles as anode for lithium ion batteries. *Micro & Nano Letters*, 10(4), 217-219. <https://doi.org/10.1049/mnl.2014.0631>
- [11] Mayeen, A., Shaji, L. K., Nair, A. K., & Kalarikkal, N. (2018). Morphological characterization of nanomaterials. In *Characterization of Nanomaterials* (pp. 335-364). Woodhead publishing. <https://doi.org/10.1016/B978-0-08-101973-3.00012-2>
- [12] Scimeca, M., Bischetti, S., Lamsira, H. K., Bonfiglio, R., & Bonanno, E. (2018). Energy dispersive X-ray (EDX) microanalysis: A powerful tool in biomedical research and diagnosis. *European Journal of Histochemistry*, 62(1), 89-99. <https://doi.org/10.4081/ejh.2018.2841>
- [13] Bindu, P., & Thomas, S. (2014). Estimation of lattice strain in ZnO nanoparticles: X-ray peak profile analysis. *Journal of Theoretical and Applied Physics*, 8, 123-134. <https://doi.org/10.1007/s40094-014-0141-9>
- [14] Hou, Q., Meng, F., & Sun, J. (2013). Electrical and optical properties of Al-doped ZnO and ZnAl<sub>2</sub>O<sub>4</sub> films prepared by atomic layer deposition. *Nanoscale research letters*, 8(1), 1-8. <https://doi.org/10.1186/1556-276X-8-144>
- [15] Choi, W., Shin, H. C., Kim, J. M., Choi, J. Y., & Yoon, W. S. (2020). Modeling and applications of electrochemical impedance spectroscopy (EIS) for lithium-ion batteries. *Journal of Electrochemical Science and Technology*, 11(1), 1-13. <https://doi.org/10.33961/jecst.2019.00528>
- [16] Belkhaoui, C., Mzabi, N., Smaoui, H., & Daniel, P. (2019). Enhancing the structural, optical and electrical properties of ZnO nanopowders through (Al+ Mn) doping. *Results in Physics*, 12, 1686-1696. <https://doi.org/10.1016/j.rinp.2019.01.085>
- [17] Sirirak, R., Phettakua, P., Rangdee, P., Boonruang, C., & Klinbumrung, A. (2024). Unveiling the impact of excessive dopant content on morphology and optical defects in carbonation synthesis of nanostructured Al-doped ZnO. *Powder Technology*, 435, 119444. <https://doi.org/10.1016/j.powtec.2024.119444>
- [18] Xie, S. H., Liu, Y. Y., & Li, J. Y. (2008). Comparison of the effective conductivity between composites reinforced by graphene nanosheets and carbon nanotubes. *Applied Physics Letters*, 92(24), 243121. <https://doi.org/10.1016/j.jallcom.2014.05.036>
- [19] Malek, M. F., Mamat, M. H., Musa, M. Z., Khusaimi, Z., Sahdan, M. Z., Suriani, A. B., ... & Rusop, M. (2014). Thermal annealing-induced formation of ZnO nanoparticles: Minimum strain and stress ameliorate preferred c-axis orientation and crystal-growth properties. *Journal of Alloys and Compounds*, 610, 575-588. <https://doi.org/10.1063/1.2949074>
- [20] Itamar, K. A. (2023). A review on nanoparticles: characteristics, synthesis, applications, and challenges. *Frontiers in microbiology*, 14, 1155622. <https://doi.org/10.3389/fmicb.2023.1155622>
- [21] Romaguera, Y., Leyet, Y., Guerrero, F., Aguilera, L., Pérez, J., & Guerra, J. D. L. S. (2009). Influence Of Bi<sup>3+</sup> Cation On Microstructure And Electrical Properties Of The ZnO Ceramics. *Revista Cubana de Química*, 21(3), 47-56.
- [22] Grewal, M. S., Kisu, K., Orimo, S. I., & Yabu, H. (2022). Increasing the ionic conductivity and lithium-ion transport of photo-cross-linked polymer with hexagonal arranged porous film hybrids. *Iscience*, 25(9), 104910. <https://dx.doi.org/10.2139/ssrn.4125674>
- [23] Ragupathi, V., Panigrahi, P., & Subramaniam, N. G. (2020, March). Enhanced electrical and optical properties of Al doped and ZnO nanoparticles for optoelectronic application: eco-friendly green route. In *Journal of Physics: Conference Series* (Vol. 1495, No. 1, p. 012040). IOP Publishing. <https://doi.org/10.1088/1742-6596/1495/1/012040>